Suppressing residual vibrations in comb-drive electrostatic actuators: a command shaping technique adapted to nomadic applications

Haythem AMEUR[a*], Patrice LE MOAL[a], Gilles BOURBON[a], Cedric VUILLEMIN[b], Marc SWOROWSKI[b]

[a] Univ. Bourgogne Franche-Comté, FEMTO-ST Institute, Department of Applied Mechanics, France

[b] SILMACH SA, Rue Sophie Germain, 25000 Besançon

[*]Corresponding author Haythem AMEUR: Département Mécanique Appliquée, 24 rue de l'épitaphe 25000 Besançon, France.

E-mail address: ameur.haythem@gmail.com ; haythem.ameur@femto-st.fr

Keywords: residual vibrations, shaping command, high voltage electrostatic actuators, nomadic applications, damping circuit

Abstract

Residual vibrations are a recurrent problem in MEMS actuators leading to a limitation of their dynamics and lifespan. This paper presents a voltage-controlled technique and its applicability to suppress residual vibrations in high voltage (about 100V) electrostatic comb-drive actuators. The studied actuator is composed of a driving module and a clutch module devoted to the step by step driving of linear or circular gears.

The proposed method is based on a command shaping technique well adapted to be integrated in an Application-Specific Integrated Circuit (ASIC), especially for nomadic applications. Firstly, an electrodynamic characterization is used to extract the key voltages of the optimized command signals. The key voltages correspond to the beginning and the end of the actual displacement. The command signals consist of two begin/end voltage jumps and a linear voltage rise/fall in an optimized time between the key voltages. Then, experimental validations investigated the influence of voltage fall time for a MEMS chip and the resulting dispersion for a set of 8 MEMS chips. The results show that residual vibrations are reduced by a factor higher than 20 in terms of the amplitude rate of bounces against back stop and the settling time of free oscillations. Finally, an analog circuit capable of building the optimized command signals is proposed and will be implemented in the next generation of the ASIC driving the electrostatic two-module actuator.

1. Introduction

Nowadays, electrostatic microelectromechanical systems (MEMS) are increasingly present in various fields and applications due to their miniaturization, low power consumption and ease of integration using silicon micromachining processing techniques. Electrostatic MEMS are widely used as sensors in a multitude of applications, but they are also used as actuators in high-end industries, e.g. switches in telecommunications [1], accelerometers in smartphones and automobiles [2], 2D and 3D micro-position in micro mirror applications [3, 4] and so on … .

Residual vibrations caused by MEMS actuations often remains a major problem that degrades system performance and reliability [1, 4, 5]. Therefore, many researches based on different damping approaches have addressed this issue in order to eliminate or at least to reduce these vibrations without losing the kinematic performance of the actuator.

Passive mechanical damping by introducing dissipative dielectric media is a solution considered to modify the dynamics of electrostatic actuators in [6, 7]. Burugupally et al. [7] develop a model describing the dynamic response of a parallel-plate actuator moving in a dissipative medium and illustrating in particular the behavior near the pull-in voltage. Schroedter et al. [6] theoretically and experimentally address the silicone oil damping on the dynamics of a vertical comb-drive. The oscillations are strongly reduced but characteristics as permittivity, refractive index and eigenfrequency of the system are largely modified.

Other works are interested in new mechanical architectures mainly implemented in gap-closing actuators [8, 9, 10]. In these cases, it is more precisely a question of pull-in instability knowing that this can also be at the origin of residual vibrations due to sudden contact as in switch applications. For example, Rivlin et al. [9] designed elastic springs with monotonically increasing stiffness counteracting the nonlinear response of the electrostatic gap-closing actuators. Such a system allows to increase the dynamic range and to force a smooth and controllable linear relation between applied voltage and resulting displacement. Abdul Rahim et al [10] consider a hybrid approach between electrical and mechanical architecture. Indeed, a dual electrode configuration is designed: one electrode is used to actuate the beam switch to the gate while an additional electrode is used to decelerate the beam to control bouncing.

However, most of the work on residual vibrations problems integrates electrical solutions because they do not affect the architecture and therefore the intrinsic kinematic properties of the system. Two main types of techniques can be distinguished: charge drive technique and voltage drive technique. Only a few works have focused on the charge control solution. Castaner et al. [11] and Choi et al. [12] perform numerical simulations of RF MEMS switches showing the possibility to reduce the energy

consumption and especially to slow down the speed during the switching phase. While the authors do not explicitly mention any benefits on potential rebounds, the slowing of the speed is necessarily favorable. Spasos et al. [13] have implemented a resistance of 33 MΩ in series with the power source to study the effectiveness of the charge drive technique to suppress residual vibrations in RF Switch. The authors point out the trade-off between vibration reduction and longer response time due to resistive damping.

On the other hand, the voltage drive technique has been more widely used according to closed-loop or open-loop control. The closed-loop control [14, 15] requires the integration of additional sensors and processing circuits, which are more expensive and complex and requires an additional delay in the response time of the system. This may be a substantial drawback in real-time applications with strong time-critical constraints such as road safety, aeronautics... This favors open-loop control, which simply consists in shaping the control signal, hence its usual calling of command shaping or also input shaping.

In [16], Chen et al. review and develop the three main types of command shapers used to control three types of electrostatic actuators: (a) linear actuators based on comb-drive structures, nonlinear actuator based on parallel plate structures either in stable (b) or pull-in (c) operation.

In the case (a) of linear actuators, the best-known command shaping suggested by Singer et al. [17] are Zero Vibration (ZV) and the Zero Vibration and Derivative (ZVD). Their principle is based on linear superposition of two-steps and three-steps sequence shaping the initial command in order to respectively obtain a zero residual vibration amplitude and in addition a zero derivative at the system eigenfrequency. Eun et al. [18] successfully applied both methods ZV and ZVD on a vertical comb-based electrostatic torsional micromirror reducing the residual vibrations (characterized by the percent overshoot) from 60% to respectively 36% and 6%. However, many other ZVD-based shapers have been investigated as “Extra-Insensitivity” and “Specified-Insensitivity” as reported in [19] in order to take into account possible deviation on eigenfrequencies.

In the case (b) of nonlinear actuators, Yin et al. [20] and Chen et al. [21] using an energy method proved theoretically and experimentally that two-steps (ZV) and three-steps (ZVD) shapers remain also efficient with amplitudes and acting time of steps different from the linear case depending in particular on initial gap. In the case (c) of nonlinear actuators as RF switches, the problem is different because it is a question of avoiding the sudden contact between mobile and fixed electrodes caused by the pull-in phenomenon. The suitable control signal is based on a three phases pulse-and-hold technique proposed in several works [22, 23]. In a first phase, an actuation pulse voltage is applied to ensure the expected displacement. In a second phase, the voltage is turn-off for a time period, so that the actuator decelerates to zero speed at the contact point. Finally, a holding voltage lower than the actuation voltage is applied to keep the mobile electrode in contact. In [24], the authors have proposed a

command shaping to handle the problem of residual vibration in both pull-in and release phases. Then, they have extended their work by the proposal of a modified shaped scheme in order to increase the robustness against parameter uncertainties. Most of the solutions put forward so far do not take into account the real conditions of industrial MEMS applications. The actuators are usually controlled by means of computer and amplifiers. In the case of real applications and especially nomadic ones, it is essential to study the feasibility of building the proposed command shapes using integrated circuits ICs from built-in batteries. In this work, an adapted shaped signal, easy to be implemented without control circuit, is presented. This makes it well suited for real MEMS applications with constraints of footprint, power consumption and cost.

The present work deals with an electrostatic actuator [25] composed of two comb-drive based modules devoted to step by step motorization of linear or circular gears. The applications envisaged are mainly nomadic motorization with a minimum footprint, e.g. for counting and/or displaying environmental or physiological data. A driving tooth is attached to both modules with decoupling elastic beams: it can be moved outwards or towards the gear by the clutch module and it can drive the gear by the driving module. Successive clutching and driving sequences allow the moving element to be driven step by step. Residual vibrations occur when the clutch or the driving module reach the end of its stroke (usually powered by electrostatic field interactions) or returns to its initial position (usually powered by elastic restoring), either freely or in a stop. These vibrations are unfavorable to proper operation because they lead to an increase of the settling times limiting the actuation frequencies, and/or they cause repeated shocks degrading the opposite surfaces and consequently the overall life of the system. Resisting torques from friction and/or unbalance, inertial loads to be driven require additional voltage compared to that needed for achieving the stroke. Moreover, the modules can be pre-stressed in particular to make easier the microfabrication process. Thus, the actual displacement takes place between two key voltages. In this context, linear schemes as ZV/ZVD are not well suited for application over the full voltage range.

In this paper, a command shaping based on a voltage drive technique is especially developed for a comb-drive based two-module actuator. Its performances in terms of residual vibrations reduction and its suitability for integration into specific integrated circuits are presented in the following sections.

Section 2 presents the actuator architecture and the context, the experimental set-up and the residual vibrations problem. Section 3 outlines the construction of the command shaping based on experimental and theoretical considerations. Section 4 is devoted to experimental validations of optimal shaping parameters for a given actuator and their relevance on a batch of actuators. In Section 5, a hardware circuit is briefly described to best satisfy the shaped signals identified in previous

sections. Lastly, conclusions are drawn on the benefits from the performances and the integration capabilities of the proposed solution and some application perspectives are discussed.

2. Residual vibration in a two-module comb-drive actuator

2.1. *Architecture and kinematics of the two-module comb-drive actuator*

Figure 1 shows the architecture of the two-module comb-drive actuator designed to drive step by step a circular gear. The actuator is fabricated by Deep Reaction Ion Etching from an SOI (Silicon on Insulator) wafer. The main steps of a similar fabrication process can be found in details in [26, 27].

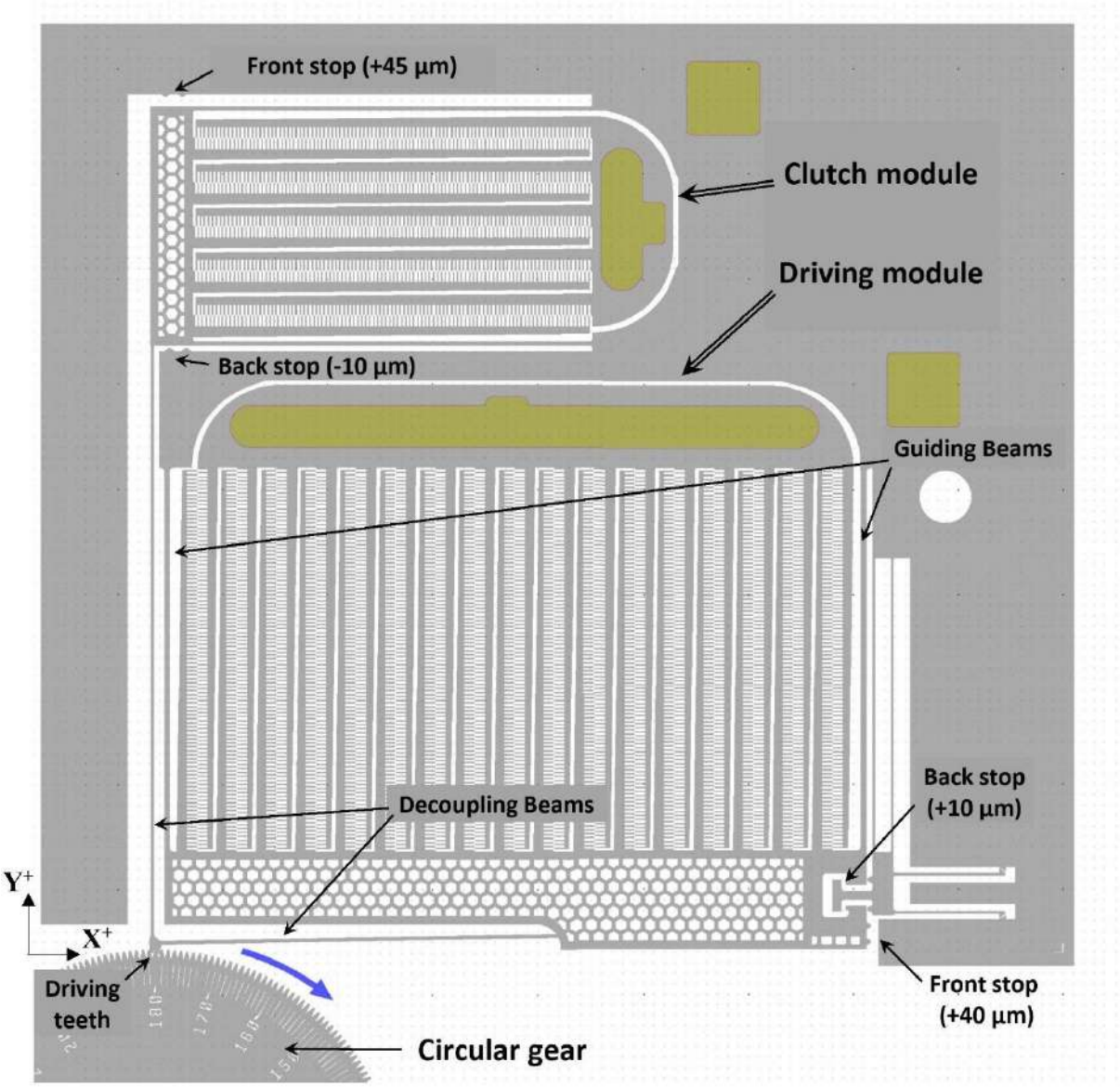

Figure 1: Layout of the two-module comb-drive actuator with the circular gear to be driven

Two driving teeth are attached to both modules by decoupling elastic beams: the driving and the clutch modules leads respectively to X and Y displacements. Both modules are made up of

interdigitated combs and elastic guiding beams respectively ensuring an "electrostatic actuated" X^+/Y^+ motion and an "elastic restored" X^-/Y^- motion of the driving teeth. As shown in Figure 1, the footprint of the driving module is larger than the clutch module one due to a greater number of interdigitated combs. Indeed, the driving module must generate a force capable of driving a moving element and thus has to overcome external loads such inertial loads or frictional forces. Table 1 reports the main mechanical and geometrical parameters of the complete actuator and especially the electrostatic force coefficient called β so that: $F_{elec} \approx \beta \, . \, V^2$ with F_{elec} the electrostatic force and *V* the voltage difference between fixed and mobile interdigitated combs. In such a comb-drive structure, "normal" (displacement-dependent, mainly between tips of comb teeth of one comb and the notch of the opposite comb) and "tangential" (displacement-nondependent, between two neighboring teeth of two opposite combs) electrostatic forces take place. However, the present comb structure has been designed so that the "tangential" forces are much larger (in a ratio from 10 to 100), so β is a constant depending only on the geometry.

	Driving Module	**Clutch Module**
Material	Single crystal silicon (100)	Single crystal silicon (100)
Footprint and thickness	3500µm x 3000µm and 200µm	2500µm x 1200µm and 200µm
Back and front stop	Δ_{back} = 10µm and Δ_{front} = 40µm	Δ_{back} = -10µm and Δ_{front} = 45µm
Balance position	$\Delta_{bal} = \Delta_{back}$ = 10µm	Δ_{bal} = 0
Total stroke	30µm → (Δ_{front}) – (Δ_{bal})	45µm → (Δ_{front}) – (Δ_{bal})
Nominal stiffness (guiding beams)	$k_{driving} \approx$ 198N/m	$k_{clutch} \approx$ 55N/m
Moving mass	$m_{driving} \approx$ 1.126mg	$m_{clutch} \approx$ 0.323mg
Electrostatic force coefficient	$\beta_{driving} \approx 0.864 \mu N/V^2$	$\beta_{clutch} \approx 0.252 \mu N/V^2$

Table 1: Main mechanical and geometrical parameters of the driving and clutch modules

At the design stage, the interdigitated combs do not overlap to facilitate etching. The driving module includes a latching mechanism which moves the mobile combs towards the fixed one by a pre-defined value. This allows the combs overlapping for a proper operating mode (driving requires a useful force from the initial position) and to have a non-zero value of the restoring force all along the "elastic restored" motion. Thus, the driving module moves between two stops located at Δ_{back} (10µm)

and Δ_{front} (40µm), i.e. a stroke of Δ_{front} - Δ_{back} (30µm). In addition, residual vibrations are translated into bounces against front stop (40µm) for the X^+ motion and against back stop (10µm) for the X^- motion.

There is no latching mechanism on the clutch module which does not require any useful force. Edge effects between non-overlapping combs initiate very gradually the declutching (more details in § 3.1). Thus, the clutch module is supposed to move between the free initial balance position (Δ_{bal} = 0µm) and the front stop (Δ_{front} = 45µm). In fact, as shown in Figure 1, a back stop (Δ_{back} = -10µm) located behind the initial position can partially limit the free oscillations. Also residual vibrations are translated into bounces against front stop (45µm) for the Y^+ motion and free oscillation down to the back stop (-10µm) for the Y^- motion.

Figure 2 illustrates the drive-clutch time sequences allowing to drive a circular gear in the clockwise direction: (0) initial position, (1) drive sequence by "electrostatic actuated" motion of the driving module, (2) declutch sequence by "electrostatic actuated" motion of the clutch module, (3) free-load back sequence by "elastic restored" motion of the driving module and (4) clutch sequence by "elastic restored" motion of the clutch module.

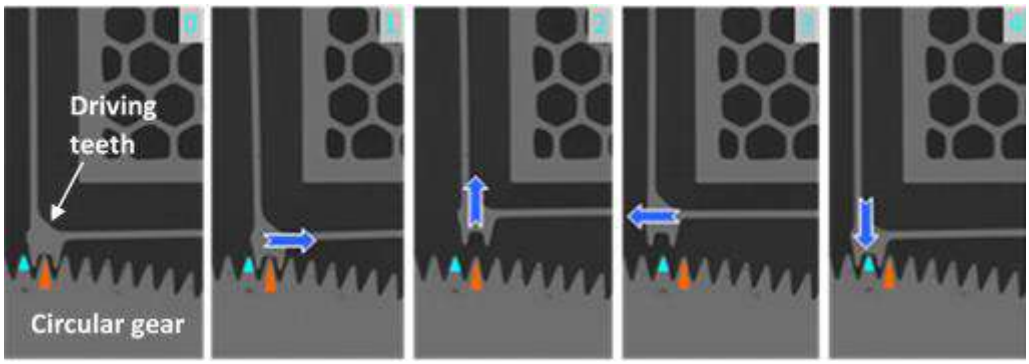

Figure 2: Chronological sequence to drive a circular gear in the clockwise direction

2.2. Experimental set-up

The manipulation consists in applying dedicated shaping signals for each module and then extracting the associated motion using a video processing technique. This latter allows ultra-fast and non-contact data acquisition with high accuracy allowing both spatial and temporal analysis. The complete instrumentation chain used in the experimental part is presented in Figure 3. First, the control signals are built from the waveform generator (Tabor 1074). The two-module comb-drive electrostatic actuator is powered by 110V voltage to ensure driving capacities, therefore electric signals from the waveform generator not exceeding $10V_{pp}$ (peak to peak) are amplified by a high voltage amplifier x 50 (Tabor 9400). Then the amplified electrical signals feed the actuator through a probe station by contacting gold pads of each module. The video acquisition is performed by a v710 PHANTOM ultra-high speed camera mounted on OLYMPUS microscope equipped with x 50 zoom.

Resolution and acquisition rate are respectively 256 x 256 pixels and 79 kframes per second. The video file is recorded by a usual computer and lastly an image analysis with TEMA® motion tracking software is performed. Thus, the current displacements of each module are tracked as a function of time and can eventually be correlated to the corresponding voltage.

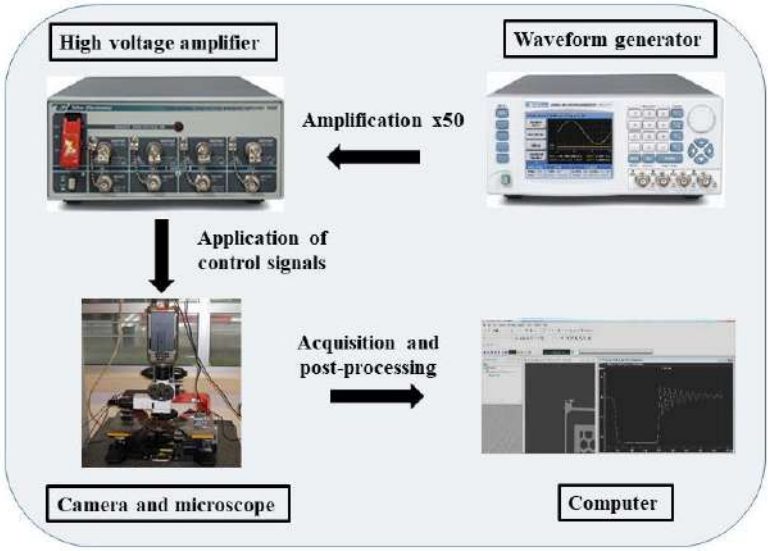

Figure 3: Instrumentation chain for the displacement tracking of the driving and clutch modules

2.3. Residual vibrations induced by unshaped signals

In order to illustrate the residual vibration problems, experiments are first conducted with unshaped signals featuring jumps in increasing or decreasing voltage. In practice, this rapid switching or jumps between two voltage values of the signals are limited by the capacities of the wave generator and here of the voltage amplifier, that are around 0.5µs/100V for the materials involved in the instrumentation chain.

The chronogram of the unshaped signals is shown in Figure 4. A time shift between driving and clutch module signals is shown to be consistent with the driving sequence. In the experiments, each module is studied separately.

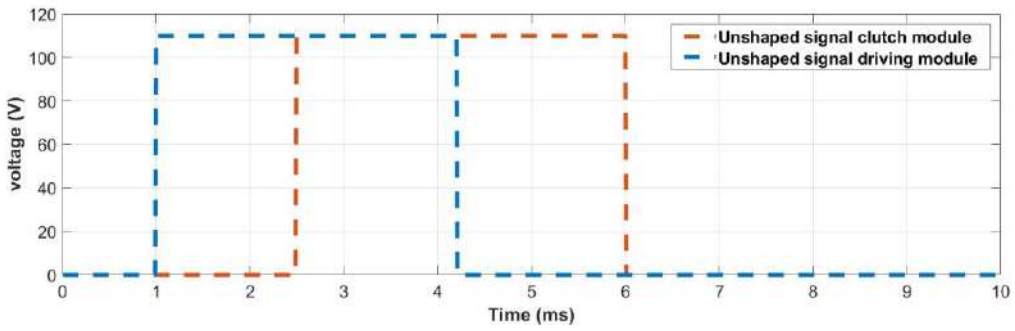

Figure 4: Chronogram of the unshaped signals for driving the two-module comb-drive actuator

Figure 5 shows the displacement responses of the driving and the clutch modules to the unshaped signals. The voltage rise and fall correspond respectively to the "electrostatic actuated" motion and the "elastic restored" motion. To analyze and quantify residual vibrations, two criteria are defined: the amplitude rate of the first bounce or oscillation compared to the total stroke called ***AR*** and the settling time $\boldsymbol{ST_{5\%}}$ to satisfy a maximal 5% amplitude rate. For the driving module, "back" bounces with ***AR*** ≈ 53% and $\boldsymbol{ST_{5\%}}$ ≈ 1ms are slightly more pronounced than "front" bounces with ***AR*** ≈ 39% and $\boldsymbol{ST_{5\%}}$ ≈ 0.53ms. For the clutch module, differences are even more striking with ***AR*** ≈ 59% and $\boldsymbol{ST_{5\%}}$ ≈ 4ms for "back" bounces and ***AR*** ≈ 30% and $\boldsymbol{ST_{5\%}}$ ≈ 0.7ms for "front" bounces".

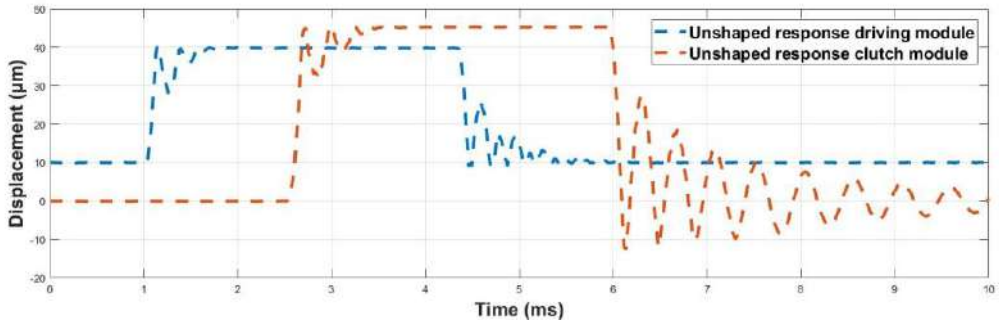

Figure 5: Mechanical responses of the two modules according to the unshaped command signals

To conclude this section, residual vibrations are clearly pointed out for unshaped signals and the resulting dynamical responses illustrate two major drawbacks. Firstly, the required chronology of the different phases necessitates a full stabilization of the previous motion before beginning the next one, and thus limits the actuation frequency. Secondly, the abrupt switching between the different positions causes significant mechanical shocks between opposing surfaces, which can rapidly degrade the driving element and consequently the performance of the actuators. In the next section, a solution based on the command shaping technique is proposed in order to improve the dynamic control of the two module comb-drive actuators in terms of amplitude rate and settling time.

3. Command shaping: key voltage features and damping times

3.1. *Electromechanical characterization: identification of key voltages in a no-load configuration*

Residual vibrations could be controlled by lengthening times of the voltage rise/fall so that it ensures a very low speed (if possible zero in theory) at the end of the movement and causes the minimum bounces or free oscillations. However, this approach may be not compatible with expected actuation frequency and/or power consumption for the intended application. The solution proposed in this work is a trade-off based on damping the voltage rises and falls only on the voltage ranges inducing an effective displacement of the two modules. In the following, the key voltage features that represent the voltage range limits are called V_{begin} and V_{end}.

Figures 6 and 7 show the electromechanical characterization of the two-module actuator in terms of X (driving module) and Y (clutch module) displacement as a function of the applied voltage. The displacement of the driving teeth is reported in a no-load configuration, i.e. without any gear to be driven. Indeed, the applied voltage is a triangular signal with a maximum voltage of 110V and a low frequency of 1Hz to avoid inertial phenomena. For both modules, the electromechanical behavior consists of three phases, both in increasing and decreasing voltage. The driving module is supposed to move between a pre-deformed value of 10µm and the front stop at 40µm. In the first phase, from 0V to V_{begin}, the electrostatic actuation force is lower than the elastic restoring force of the pre-deformed guiding beams and thus no displacement occurs. At V_{end}, the driving module contact the front stop and logically no further displacement is possible. Thus, the effective displacement takes place between V_{begin} around 45V and V_{end} around 97V. In Figure 7, the behavior of the clutch module is slightly different during the first phase between 0V and V_{begin}. It is recalled that in this work, the clutch module is not pre-deformed and have non-overlapped fixed and mobile combs. Before the actual overlap of combs, electrostatic interactions are due to edge effects and not to usual tangential parallel-plate electrostatic forces. Thus, in the first phase, the displacement is not zero but evolves very weakly in increasing or symmetrically in decreasing voltage. As shown in Figure 7, the corresponding voltage V_{begin} is identified around 35V at the intersection of the tangents of the curves representing the first and second phases. In the same way as for the driving module, the clutch module contacts the front stop at V_{end} around 99V.

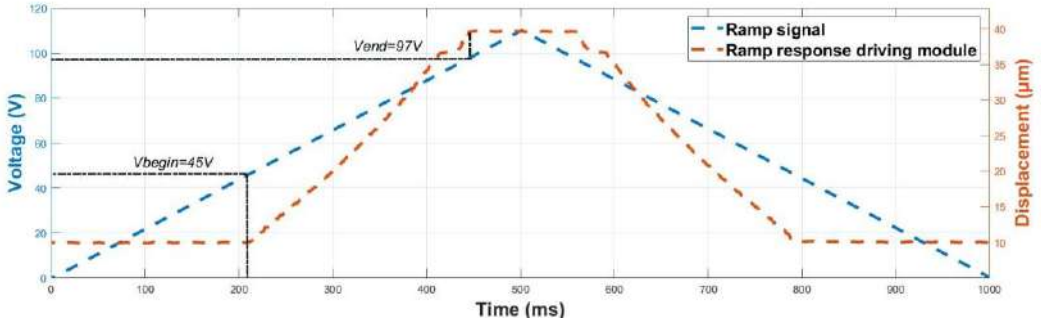

Figure 6: Electromechanical characterization of the driving module displacement as function of voltages

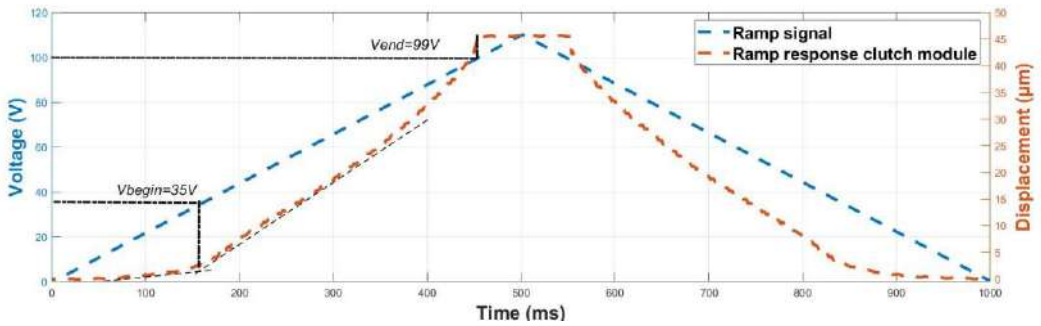

Figure 7: Electromechanical characterization of the clutch module displacement as function of voltages

3.2. Shaped command signals: general case, specificity of the "electrostatic actuated" motion and theoretical estimation of the voltage fall time for the "elastic restored" motion

3.2.1.General case

Figure 8 illustrates the new chronogram with the shaped command signals. Considering for example the rise in voltage, each command signal consists in an abrupt switching between 0V and V_{begin}, a voltage ramp between V_{begin} and V_{end} with a time rise τ to be determined and a last abrupt switching between V_{end} and V_{MAX} (i.e. 110V). The shaped command signal for the fall in voltage is the symmetrical one. Although the voltage ramp is the actual only damping phase, voltage jumps are important. On the one hand, the first jump avoids having to maintain the V_{begin} voltage during the rest phases, which could be a source of power consumption (leakage of electric charges). On the other hand, the second jump is related to the additional voltage required to overcome resisting torques to drive the gear.

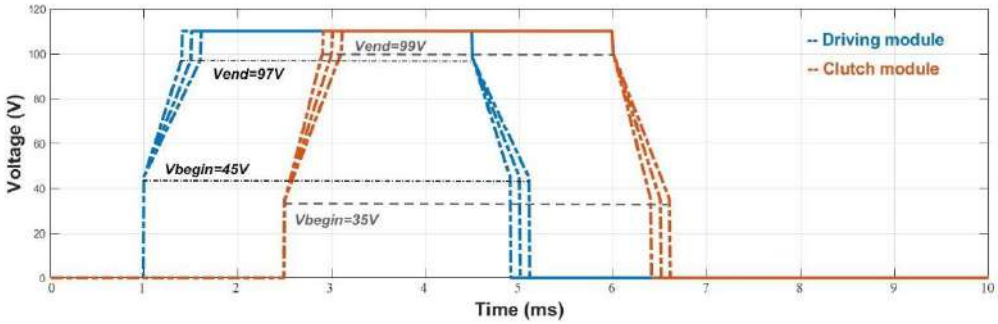

Figure 8: New chronogram with shaped command signals for the two-module comb-drive actuator

In the proposed application, the constraints on the rise time or the fall time τ are different depending on the corresponding motion, either the "electrostatic actuated" motion or the "elastic restored" motion.

3.2.2. Specificity of the "electrostatic actuated" motion

The targeted applications concern preferably the motorization of mechanical elements in portable devices. Therefore, ASICs are used to control and to power the two-module actuators. These circuits integrate in particular voltage multiplier stages (one per module) in order to reach voltages of the order of 100V from a button cell of 1.5V or 3V. In [28], such a voltage multiplier stage is rapidly described: i.e. an integrated charge pump characterized by an average rise time about 0.8ms to reach a voltage of 110V from 3V. To illustrate this problem, the previous experimental set-up is used to generate a linear voltage rise from 0V to 110V in 0.8ms. Figures 9a and 9b show the resulting displacement in three cases: unshaped command, shaped command (τ is about 0.5ms which is in the optimal range, see §4 on Experimental results) and simulated command charge pump. Thus, the rise

time about 0.8ms is slow enough so that residual vibrations do not occur in “electrostatic actuated” motions for both driving and clutch modules. Thus, the relevance of a command shaping must be evaluated in relation to the possible applications and especially to the means of integration of the solution. Moreover, the damping due to the charge pump during the “electrostatic actuated” motion justifies the identification of the key voltages in a no-load configuration. This is the case of the free back motion of the driving module corresponding to the “elastic restored” motion. However, the problem for the “elastic restored” motion remains unresolved because the charge pump is usually cut off and a sudden drop in voltage takes place.

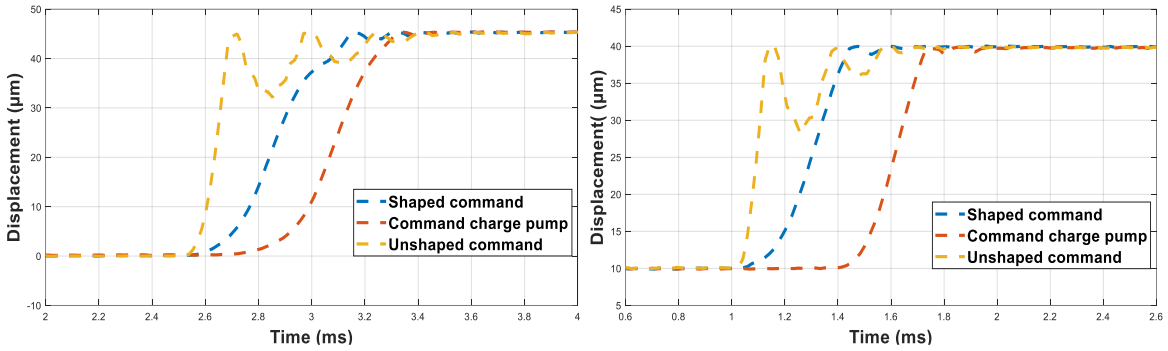

a) *b)*

Figure 9: Resulting motion from a typical electrical signal delivered by an integrated charge pump: a) Displacement of the driving module, b) Displacement of the clutch module

3.2.3. Theoretical estimation of the voltage fall time for the “elastic restored” motion

The modal analysis of the two-module structure with ANSYS® software shows that the lowest mode of resonance around 2kHz is the rigid body displacement of the mobile combs controlled by the spring effects of the flexible guiding beams. The first next resonance mode is related to the bending modes of the combs around 11kHz. Thus, due to the frequency gap, both modules can be simply modeled by a unidimensional mass-spring-damper model with the following parameters: $m_{driving}$ or m_{clutch} the mobile mass (mobile combs and support / driving teeth) of the driving or clutch module, $k_{driving}$ or k_{clutch} the bending stiffness of the guiding beams of the driving or clutch module and α the damping coefficient. Figures 10a and 10b show a schematic representation of possible final configurations of the driving and clutch modules in the “elastic restored” phase during the voltage fall. In Figure 10a, the final balance position of the driving module is a pre-stressed one by the back stop (the spring is compressed matching the guiding beams are bent). In Figure 10b, the final balance position of the clutch module is a free one (the spring is free matching the free-stress guiding beams).

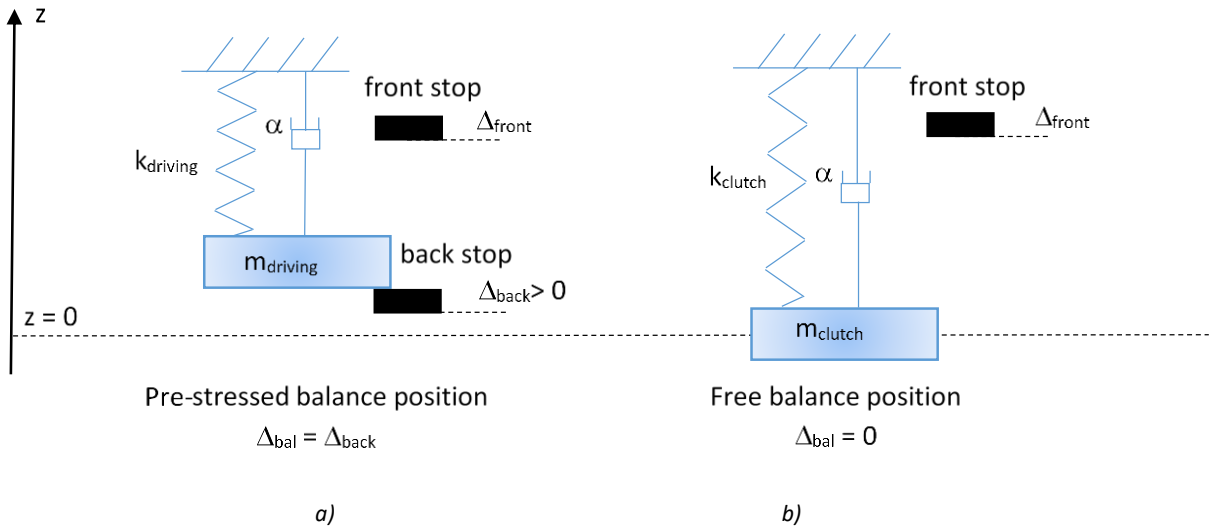

Figure 10: Schematic representation at the end of the "elastic restored" motion (a) Final position of the driving module against the back stop at Δ_{back} = 10µm (b) Final position of the clutch module at the balance position at Δ_{bal} = 0

It is a question of limiting the bounces against the stops in the case of Figure 10a and the free oscillations around the balance position in the case of Figure 10b, whatever the nature of the module involved. For example, the clutch module may also be pre-deformed by the moving element after assembly in an actual application. Optimally to cancel the bounces against the stops or the free oscillations, the voltage fall must be such that the speed of the module must be zero at the corresponding balance position. This balance position is the back stop location for Figure 10a, i.e. $\Delta_{bal} = \Delta_{back}$ and the natural balance position of the guiding beams for Figure 10b, i.e. $\Delta_{bal} = 0$.

Until the stop is reached, the mechanical behavior is linear and the fundamental relation of dynamics applied to the mass-spring-damper model gives:

$$\ddot{z} + 2\alpha\omega_n\dot{z} + \omega_n^2 z = \frac{F_{elec}}{m} = \frac{\beta}{m} \cdot V^2(t) \quad (1)$$

with z the X- or Y- displacement, β the electrostatic force coefficient (not dependent on the displacement) and α the damping coefficient and ω_n the natural pulsation $\left(\omega_n = \sqrt{\frac{k}{m}}\right)$.

According to the above, the voltage is supposed to linearly decrease between V_{end} to V_{begin}. However, inertial effects may affect V_{begin} and in order to deduce intrinsic information on the fall time, the following form is considered for the evolution of the voltage:

$$V(t) = V_{end} - \lambda \cdot t \quad (2)$$

with λ the slope of the voltage fall and $V_{end} = \sqrt{\frac{k\Delta_{front}}{\beta}}$.

The solution of the second order differential equation (1), based on the initial conditions $z(t_0 = 0) = \Delta_{front}$ and $\dot{z}(t_0 = 0) = 0$, can be written in the following form:

$$z(t) = e^{-\alpha\omega_n t}(a\cos\omega t + b\sin\omega t) + a_0 + a_1 t + a_2 t^2 \quad (3)$$

with the coefficients a_0, a_1, a_2 depending in particular on the slope λ describing the particular solution of the second order differential equation and a, b depending on the initial conditions. τ_{th} is assumed to be the time so that the corresponding position $z(\tau_{th})$ is equal to the balance position (pre-stressed Δ_{back} or free 0) and the speed $\dot{z}(\tau_{th})$ is zero. Since the beginning time t_0 is zero, τ_{th} is also the expected duration of the optimal voltage fall.

Thus, the problem consists in solving the following nonlinear two-equation system with two unknowns which are the fall time τ_{th} and the slope λ of the voltage fall:

$$\begin{cases} z(\tau_{th}) = e^{-\alpha\omega_n\tau_{th}}(a\cos\omega\tau_{th} + b\sin\omega\tau_{th}) + a_0 + a_1\tau_{th} + a_2{\tau_{th}}^2 = \Delta_{bal} = \begin{cases}\Delta_{back}\\ or\\ 0\end{cases} \\ \dot{z}(\tau_{th}) = e^{-\alpha\omega_n\tau_{th}}[(-\alpha\omega_n a + b\omega)\cos\omega\tau_{th} + (-\alpha\omega_n b - a\omega)\sin\omega\tau_{th}] \\ \qquad\qquad +a_1 + 2a_2\tau_{th} = 0 \end{cases} \quad (4)$$

The damping coefficient can be estimated at approximately 4% by the well-known logarithmic decrement method from the free oscillations of the clutch module in Figure 5. However, this coefficient can fluctuate depending on external conditions (such as ambient pressure), so the numerical solution of this nonlinear system is performed according to a realistic range of damping coefficients α from 0% to 10%. The nominal parameters of the driving and clutch modules in terms of mass, stiffness, front stop and balance positions are reported in Table 1. Figures 11 give the evolution of the displacement and the speed in the case of both driving and clutch modules for the nominal parameters. This illustrates in the case of the optimal voltage fall time the damping of the displacement with a speed that decreases sharply at the beginning, reaches a minimum, then increases and becomes zero at the location of the pre-stressed or free balance position as expected. Given the balance position and the zero speed conditions, the system theoretically remains in equilibrium thereafter.

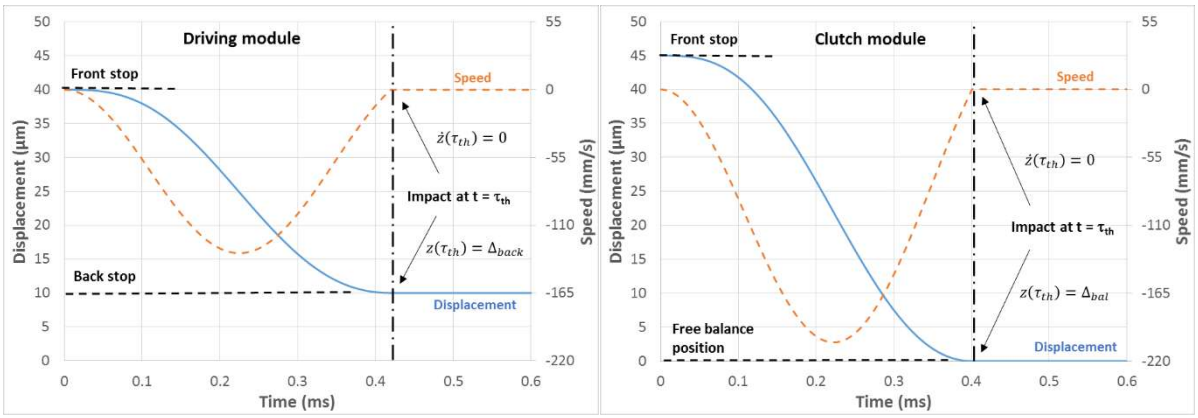

a) b)

Figure 11: Evolution of the displacement and the speed in the case of the driving module (a) and the clutch module (b) for the optimal voltage fall time

Figures 12a and 13a show the evolutions of the voltage fall time τ_{th} for the nominal parameters of the driving and clutch modules. Two additional stiffness values (half and double the nominal) and the balance position of the other module are also simulated to give the trends of their respective influences. These left Figures 12a and 13a indicate that the damping coefficients and the balance positions (at least in the range studied) have rather little impact on the fall time. Conversely, the higher the stiffness, the shorter the fall time required. On the other hand, the plot of the evolution of the fall time normalized by the corresponding natural period, i.e. τ_{th} / T $\left(T = 2\pi\sqrt{\frac{m}{k}}\right)$, show on the right Figures 12b and 13b a non-dependence with respect to the considered stiffness. All the related colored lines overlap perfectly. Thus, the normalized fall time for all the studied configurations is in the 81% - 97% range.

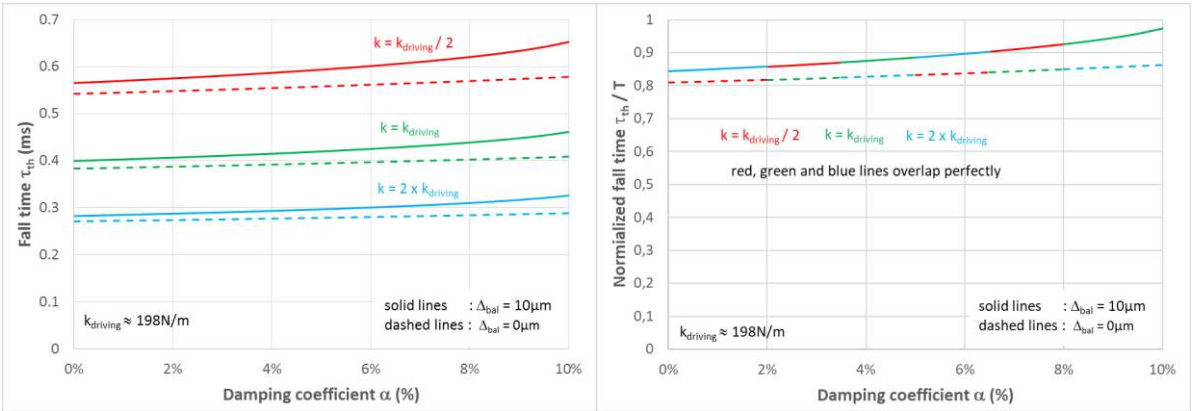

a) *b)*

Figure 12: Evolution of the fall time τ_{th} as a function of the damping coefficient a) and corresponding evolution of the normalized fall time τ_{th}/T b) based on nominal parameters of the driving module

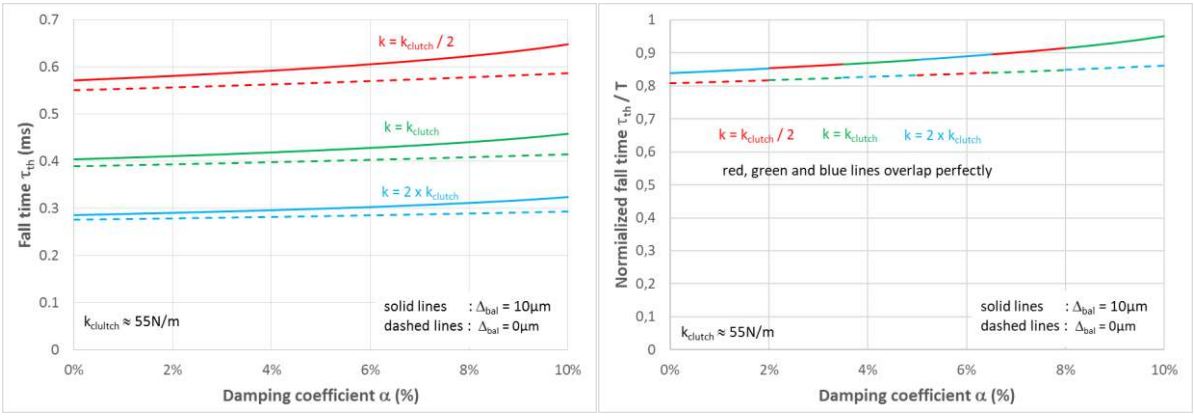

a) *b)*

Figure 13: Evolution of the fall time τ_{th} as a function of the damping coefficient a) and corresponding evolution of the normalized fall time τ_{th}/T b) based on nominal parameters of the clutch module

4. Experimental validation of command shaping and hardware solution

4.1. *Experimental investigations on the voltage fall time: optimum and robustness*

The theoretical estimation presented above according to a simple analytical approach concludes to a voltage fall time of the order of 81% - 97% of the natural period of the considered module. As the natural periods of the two modules are very close around 0.48ms, many experimental tests are conducted in a range around 0.30ms – 0.62ms. Figure 14 shows the main results obtained with a special focus around 0.4ms (0.37ms – 0.41ms) and 0.5ms (0.51ms – 0.55ms) respectively for the driving and clutch modules.

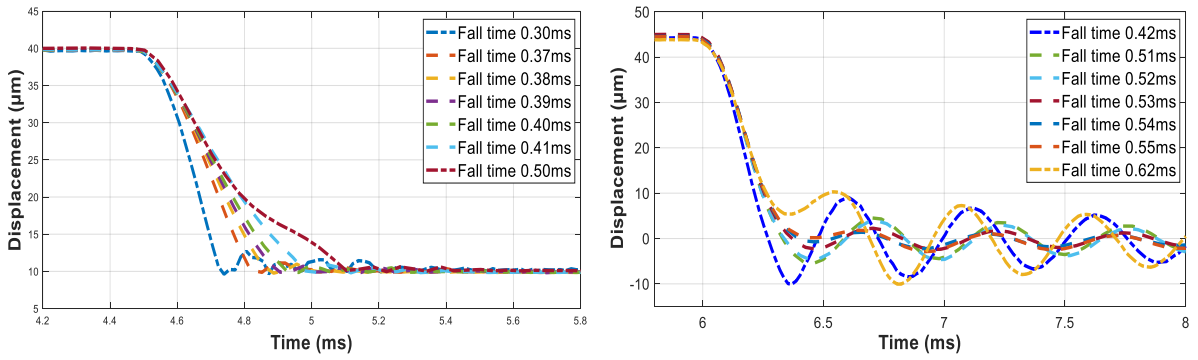

a) *b)*

Figure 14: Influence of the voltage fall time in the "elastic restored" motion in the case of a) the driving module and b) the clutch module

The amplitude rate ***AR*** and the settling time $\boldsymbol{ST_{5\%}}$ previously defined are reported in Table 2 for the investigated ranges. Table 2 shows optimum values in terms of decrease factor of ***AR*** and $\boldsymbol{ST_{5\%}}$ compared to the unshaped command performances:

- τ_{exp} = 0.39ms for the driving module with a decrease factor of $\mathbf{22.6_{AR}}$ and $\mathbf{2.6_{ST5\%}}$,

- τ_{exp} = 0.53ms for the clutch module with a decrease factor of **14.0**$_{AR}$ and **9.1**$_{ST5\%}$.

Module	Fall time (ms)	*AR*	$ST_{5\%}$	Module	Fall time (ms)	*AR*	$ST_{5\%}$
Driving module	0.30	8.99%	0.54ms	**Clutch module**	0.42	21.3%	≈ 4ms
	0.37	3.73%	0.34ms		0.51	9.7%	2.16ms
	0.38	3.23%	0.38ms		0.52	6.1%	0.78ms
	0.39	2.34%	0.39ms		0.53	4.2%	0.44ms
	0.40	2.69%	0.42ms		0.54	5.1%	0.75ms
	0.41	2.88%	0.48ms		0.55	7%	1.32ms
	0.50	---	0.58ms		0.62	23.9%	≈ 4ms

*Table 2: Amplitude rates **AR** and settling times $ST_{5\%}$ from experimental implementation of command shaping*

Moreover, the ranges of values investigated underline a certain robustness of the command shaping. Considering a deviation of +/- 0.02ms from the optimum values (i.e. a relative deviation +/- 5%), Table 2 shows a minimum decrease factor of ***AR*** and $ST_{5\%}$ as follows:

- τ_{exp} = 0.37ms – 0.41ms for the driving module, a minimum decrease factor of **14.2**$_{AR}$ and **2.1**$_{ST5\%}$,
- τ_{exp} = 0.51ms – 0.55ms for the clutch module, a minimum decrease factor of **6.1**$_{AR}$ and **1.9**$_{ST5\%}$.

Thus, the dynamic behavior of the driving module is not very sensitive to the voltage fall time since a deviation of +/- 0.1ms, i.e. a relative deviation higher than 20% maintains a good efficiency (decrease factor of **5.9**$_{AR}$ and **1.9**$_{ST5\%}$). The pre-stressed balance position against the back stop appears to be a mechanical condition that significantly favors the robustness of the command shaping.

On the contrary, the clutch module, that satisfies a free balance position, is much more sensitive to the voltage fall time. Indeed, the same deviation of +/- 0.1ms provides a decrease factor of about **2.5**$_{AR}$ and the settling time $ST_{5\%}$ is not decreased compared to the unshaped command. In reality, a damping effect remains since the amplitude ratio ***AR*** decreases but the 5% threshold considered for $ST_{5\%}$ is not affected.

To conclude, the experimental results highlight optimal values allowing to reduce significantly the residual vibrations but also the robustness of the command shaping on relative value ranges of 5% on

either side of the optimal value. Furthermore, the experimental value ranges are very close to the numerical estimations justifying the simple theoretical approach to limit the value range of experimental investigations on optimum.

4.2. Dispersion on a set of 8 MEMS

A set of 8 identical MEMS is picked up from the same wafer (including 900 chips in total) at different locations for evaluating the results dispersion for a given voltage fall time. Figure 15 shows the obtained results for the clutch and driving modules in the case of the optimal voltage fall time of 0.53ms and 0.39ms. The chip number 2 corresponds to the previously studied MEMS in §4.1.

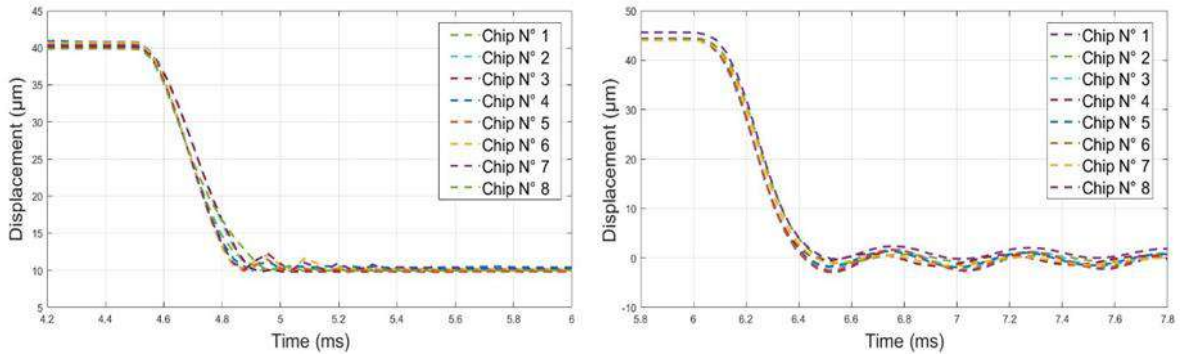

a) *b)*

Figure 15: Dynamic behavior of a set of 8 MEMS chips in the "elastic restored" motion in the case of a) the driving module and b) the clutch module

The same dynamics can be observed in the mechanical response of the two modules for the 8 chip tested. In the case of the clutch module, the amplitude rates ***AR*** and the settling times $ST_{5\%}$ obtained are respectively between 3.5% and 4.9% and between 0.42ms and 0.44ms. A similar variation for both ***AR*** and $ST_{5\%}$ is noted for the driving module, i.e. minimum decrease factors around $\mathbf{15_{AR}}$ and $\mathbf{2_{ST5\%}}$. In the previous paragraph, the geometry is fixed and the voltage fall time τ varies, here τ is fixed and the geometry potentially varies, and as a consequence the key voltages. The experimental characterization of the key voltages V_{end} and V_{begin} for the set of 8 chips gives an average deviation of about +/- 2V from the nominal values of the chip n° 2 reported in Figures 6 and 7. This means that the proposed shaped command remains efficient in a relative range of about +/- 2% and +/- 5% respectively around the nominal values of V_{end} and V_{begin}.

Thus, the experimental results prove the efficiency and a form of robustness of the proposed shaped command. It is understood, in this study, the robustness of the command is partly related to the actuator architecture and microfabrication process. However, the comb actuator architecture and standard deep-etching process can be generic to many applications. Subsequently it allows to consider

a hardware solution for practical applications. Thereafter, the hardware solution that generates the proposed control signals is called damping circuit.

4.3. Hardware architecture of the damping circuit

The originality of the hardware solution lies in the construction of the voltage fall signal which consists in an adapted and very weakly power-consuming management of the capacitive actuator discharge to damped the "elastic restored" motion. In practice, the two-module actuator is driven by an Application-Specific Integrated Circuit (ASIC). The ASIC includes charge pumps able to generate 110V output voltage from a 3V lithium battery. The main blocks of the ASIC are presented in Figure 16 and consist of:

- Low voltage digital core to manage the charge pumps and high voltage switches,
- Charge pumps including a voltage regulator to generate high voltage signals,
- High voltage (HV) switches to connect the MEMS either to the damping circuit or to the charge pump outputs,
- VDD Bootstrap Circuit to drive the damping circuit,
- A damping circuit makes it possible to generate voltage drops in the form of the proposed control signals (see Figure 8).

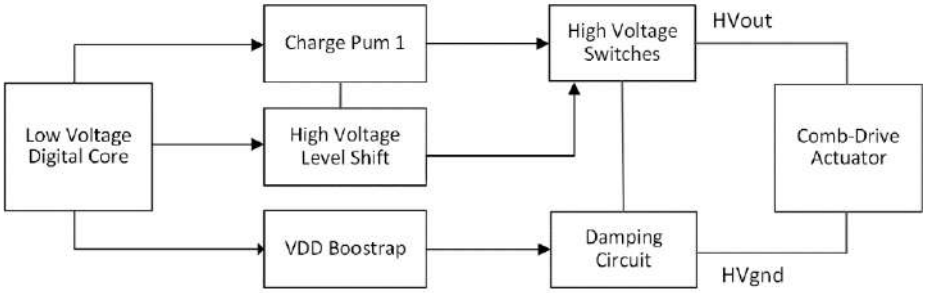

Figure 16: Block diagram of the MEMS control circuit

In the following, it is focused on the functionality of the damping circuit for an elementary module of the comb-drive actuator, taking the case of the driving module. The damping block contains a Zener diode, a resistor and an N-channel MOSFET transistor, as shown on the left in Figure 16.

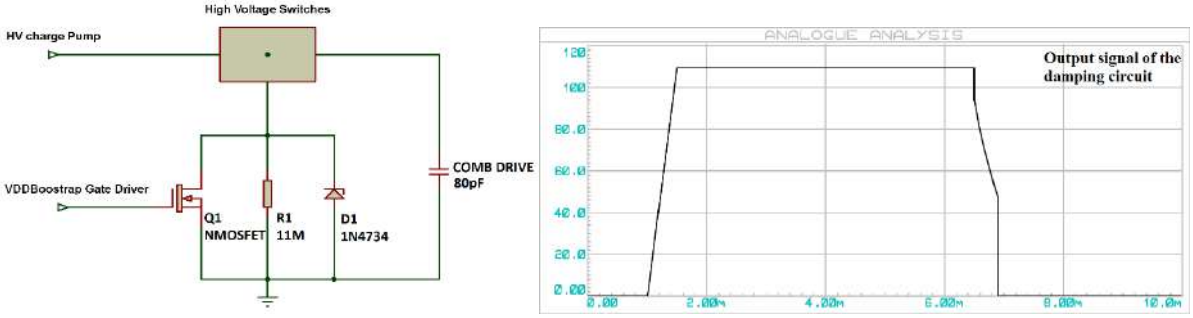

Figure 17: Damping circuit design and its output signal

Considering that the HV switches block connects the driving module to the damping circuit. Initially the actuator is charged at *110V*, subsequently the damping module operates as follows:

- In a first phase, the VDD Boostrap gate driver blocks the N-channel MOSFET transistor with the control signal HVgnd. The electric charges accumulated in the comb-drive are rapidly discharged by the Zener diode up to its threshold voltage, which in this case is identified at the V_{end} voltage (i.e. *97V*). Below the threshold voltage, the resistor takes over to continue the discharge by dissipating the mechanical energy. The evacuation of electric charges slows down considerably and the voltage gradually decreases.

- In a second phase, the VDD Boostrap gate driver activates a VDD control signal to the N-channel MOSFET transistor. This latter will pass and electric charges are rapidly evacuated through the HVgnd. The switching of the VDD Boostrap control voltage takes place after a delay of 0.39ms (corresponding to the optimal τ) from the beginning of the discharge cycle. Therefore, the value of the discharge resistance should be chosen so that V_{begin} voltage (i.e. 45V) is reached at this point. The final constructed signal is presented on the right in figure 17.

The proposed shaped signal is easy to implement and does not require specific control circuits. The presented simple hardware architecture is able to generate the appropriate command shaping for the two-module comb-drive actuator using very few components and low electrical energy consumption, what makes the system well suited to industrial applications with energy and surface constraints. In fact, the damping circuit is not connected to the charge pump, which is the power source of the system. The damping circuit will be only activated during a very limited period of the damping phase and will be directly supplied by the electrical charges accumulated in the comb-drive. The additional current, that can be consumed by the system, is the leakage current required to drive the MOSFET transistor.

5. Conclusion

In this work, a voltage-controlled technique to strongly reduce residual vibrations in electrostatic comb-drive based actuators is presented. Residual vibrations are at the origin of an actuation frequency limitation and especially a premature wear of the elements coming in contact during the driving and clutching phases. The approach consists in applying a command shaping only in the effective displacement range and for a given duration. The method starts with an electromechanical characterization phase in order to well define the dynamic behavior of the two modules and more particularly the effective displacement range described by two key voltage values V_{begin} and V_{end}. A

simple theoretical approach based on a mass-spring-damping model shows that there is an optimal range for voltage fall time about 80% - 100% of the natural frequency of the corresponding modules.

It is shown from several experimental tests that the command shaping is efficient in a range of +/- 5% around the optimal voltage fall time; i.e. a minimum decrease factor of **14.2_{AR}** and **$2.1_{ST5\%}$** for the driving module and a minimum decrease factor of **6.1_{AR}** and **$1.9_{ST5\%}$** for the clutch module. Thus, the command seems to be quite robust with respect to the voltage fall time, in particular to reduce the amplitude rate of bounces against back stop which is a key point to improve actuator lifetime.

Moreover, the method remains very effective on a set of 8 MEMS chips picked up from a same wafer providing response elements for the sensitivity of the shaped command to deviations of the key voltages V_{begin} and V_{end}. In this study, the robustness of the command is experimentally discussed and is partly related to the actuator architecture and the microfabrication process. Indeed, microfabrication uncertainties influence geometrical parameters with possibly opposite consequences: for example, over-etching increases electrostatic gaps; i.e. increases the key voltages and decreases the width of guiding beams; i.e., decreases the key voltages.

The originality of this work is that the command solution is investigated according to real applications and especially to nomadic applications involving high voltage (about 100V) electrostatic actuators. First, the damping of the “electrostatic actuated” motion is intrinsically solved by the charge pump required for the voltage amplification. Then, the damping of the “elastic restored” motion is achieved by the management of capacitive actuator discharge. This makes it well suited for real MEMS applications with constraints of mechanical performances (about tens of volts), power consumption, footprint and cost. Moreover, these points are strongly tied since the operating voltage determines the control circuit and the power source, which influences the power consumption, the footprint of the circuit and obviously the cost that highly depends on the footprint in a batch fabrication process.

Currently, experimental life testing over millions of operating cycles is underway to validate the resulting reduction in wear and increase in life of comb-drive electrostatic actuators. Due to their micrometer steps, a large number of cycles are expected for MEMS applications aiming at perceptible effects at the human scale. For example, the motorizing of gears makes it possible to consider nomadic applications derived from watchmaking; such as counters and displays of environmental or physiological parameters. Due to the possible limitations of mechanical performances available on MEMS, optical applications could be preferred as beam shutter or deviation, control of micro-mirror arrays. However, more specific applications that do not concern the human scale can be put forward such as laboratory instrumentation. For example, micropositioning under a microscope may require fast and stabilized actuations. This is not a nomadic application but the electrical supply by external wires can be problematic if no integrated solution is proposed as it is the case in this work.

Acknowledgements: This work was funded by the European program FEDER, NEXT WATCH and was partly supported by the french RENATECH network and its FEMTO-ST technological facility.

Bibliographies:

[1] T. Cao, T. Hu, Y. Zhao, "Research Status and Development Trend of MEMS Switches: A Review", Micromachines, 11, 694, 2020.
doi:10.3390/mi11070694.

[2] W. Niu, L. Fang, L. Xu, X. Li, R. Huo, D. Guo, Z. Qi, « Summary of Research Status and Application of MEMS accelerometers », Journal of Computer and Computations, 6, 215-221, 2018.
doi: 10.4236/jcc.2018.612021

[3] M. Imboden, J. Chang, C. Pollock, E. Lowell, M. Akbulut, J. Morrison, T. Stark, D.J. Bishop, "High-Speed Control of Electromechanical Transduction: Advanced Drive Techniques for Optimized Step-and-Settle Response of MEMS Micromirrors" in IEEE Control Systems Magazine, vol. 36, no. 5, pp. 48-76, Oct. 2016.
doi: 10.1109/MCS.2016.2584338.

[4] F. Ceyssens, S. Sadeghpour, H. Fujita, R. Puers, "Actuators: Accomplishments, opportunities and challenges", Sensors and Actuators A: Physical, Vol. 295, 2019, 604-611, ISSN 0924-4247,
doi : 10.1016/j.sna.2019.05.048.

[5] K.S. Ou, K.S. Chen, T.S. Yang, S.Y. Lee, « Fast Positioning and Impact Minimizing of MEMS Devices by Suppression of Motion-Induced Vibration by Command-Shaping Method", Journal of MicroElectroMechanical Systems, vol. 20, N° 1, 2011.
doi:10.1109/JMEMS.2010.2100023.

[6]R. Schroedter, J. Grahmann, K. Janschek, "Silicone Oil Damping for Quasi-static Micro Scanners with Electrostatic Staggered Vertical Comb Drives", IFAC-PapersOnLine, Volume 52, Issue 15, 2019, Pages 37-42, ISSN 2405-8963,
doi:10.1016/j.ifacol.2019.11.646.

[7] S.P. Burugupally, W. Roshantha Perera." Dynamics of a parallel-plate electrostatic actuator in viscous dielectric media", Sensors and Actuators A: Physical, Vol. 295, 366-373, 2019.
doi: 10.1016/j.sna.2019.06.005

[8] M. Shavezipur, P. Nieva, S.M. Hashemi, A. Khajepour, "Linearization and tunability improvement of MEMS capacitors using flexible electrodes and nonlinear structural stiffness", Journal of Micromechanics and Microengineering, vol. 22, n° 2, 2012. doi:10.1088/0960-1317/22/2/025022.

[9] B. Rivlin, D. Elata, "Design of nonlinear springs for attaining a linear response in gap-closing electrostatic actuators", International Journal of Solids and Structures, Vol. 49, Issue 26, 3816-3822, 2012.
doi: 10.1016/j.ijsol.str.2012.08.014

[10] F. Abdul Rahim, M.I. Younis, "Control of bouncing in MEMS switches using double electrodes", Mathematical Problems in Engineering, 10 pages, 2016.
doi: 10.1155/2016/3479752.

[11] L. M. Castaner, S. D. Senturia, "Speed-Energy Optimization of Electrostatic Actuators Based on Pull-In", Journal of MicroElectroMechanical Systems, vol. 8, n° 3, pp. 290-298, 1999, doi: 10.1109/84.788633.

[12] K.H. Choi, et al. "Simulation of Constant-Charge Biasing Integrated Circuit for High Reliability Capacitive RF MEMS Switch." (2008).

[13] M. Spasos, R. Nilavalan, "Resistive damping implementation as a method to improve controllability in stiff ohmic RF-MEMS switches", Microsystem Technology, 19, 1935–1943, 2013.
doi: 10.1007/s00542-013-1757-4

[14] L. Dong, J. Edwards, "Closed-loop Voltage Control of a Parallel-plate MEMS Electrostatic Actuator", Proceedings of the 2010 American Control Conference, Baltimore MD, USA,30 june-2 july 2010.
doi: 10.1109/ACC.2010.5531118

[15] B. Borovic, C. Hong, X.M. Zhang, A.Q. Liu, F.L. Lewis, "Open vs. Closed-Loop Control of the MEMS Electrostatic Comb", Proceedings of the 2005 IEEE International Symposium on, Mediterrean Conference on Control and Automation Intelligent Control, Limassol, Cyprus, 27-29 june 2005.
doi: 10.1109/.2005.1467147

[16] K.S. Chen, K.S. Ou, "Command-Shaping Techniques for Electrostatic MEMS Actuation: Analysis and Simulation", Journal of MicroElectroMechanical Systems, vol. 16, n° 3, pp. 537-549, 2007.
doi: 10.1109/JMEMS.2007.893512

[17] N.C. Singer, W.P. Seering, "Preshaping Command Inputs to Reduce System Vibration", Journal of Dynamic Systems, Measurement, and Control, 112 (1), 76-82, 1990.
doi: 10.1115/1.2894142

[18] Y. Eun, B. Jeong, J. Kim, « Switching Time Reduction for Electrostatic Torsional Micromirrors Using Input Shaping », Japanese Journal of Applied Physics, 49, 2010.
doi: 10.1143/JJAP.49.054102

[19] W.E. Singhose, "Command Shaping for Flexible Systems: A Review of the First 50 Years" International Journal of Precision Engineering and Manufacturing, Vol. 10, n° 4, pp. 153-168, 2009.
doi: 10.1007/s12541-009-0084-2

[20] J.F. Yin, "Development of nonlinear input shaping methods and its application on residual vibration suppression of electro-mechanical systems", M.S. Thesis, National Cheng-Kung University, Tainan, Taiwan, R.O.C., 2004.

[21] K.S. Chen, T.S. Yang, J.F. Yin, "Residual Vibration Suppression for Duffing Nonlinear Systems With Electromagnetical Actuation Using Nonlinear Command Shaping Techniques", Journal of Vibration and Acoustics, Vol. 128, n° 6, pp. 778-789, 2006.
doi: 10.1115/1.2203340

[22] H. Sumali, J.E. Massad,D.A. Czaplewski, C.W Dyck, "Waveform design for pulse-and-hold electrostatic actuation in MEMS", Sensors and Actuators A, Vol. 134, pp213-220, 2007.
doi: 10.1016/j.sna.2006.04.041

[23] D. A. Czaplewski, C.W. Dyck, H. Sumali, J.E. Massad, J.D. Kuppers, I. Reines, W.D. Cowan, C.P. Tigges, "A Soft-Landing Waveform for Actuation of a Single-Pole Single-Throw Ohmic RF MEMS Switch", Journal of MicroElectroMechanical Systems, vol. 15, n° 6, pp. 1586-1594, 2006.
doi: 10.1109/JMEMS.2006.883576

[24] Ou, Kuang-Shun, Kuo-Shen Chen, Tian-Shiang Yang and Sen-Yung Lee. "A command shaping approach to enhance the dynamic performance and longevity of contact switches." Mechatronics 19 (2009): 375-389.
DOI:10.1016/J.MECHATRONICS.2008.09.009

[25] G. Bourbon, C. Hibert, E. Joseph, P. Le Moal, P. Minotti, « Method of producing a MEMS device », European Patent, EP 1 599 766, date of issue: 05.08.2013.

[26] Y.M. Eltagoury, M. Soliman, Y.M. Sabry, M.J. Alotaibi, D. Khalil, "Electrostatic Comb-Drive Actuator with High In-Plane Translational Velocity", Micromachines, 7, 188, 2016.
doi: 10.3390/mi7100188

[27] K. Laszczyk, S. Bargiel, C. Gorecki, J. Krezel, P. Dziuban, M. Kujawinska, D. Callet, S. Frank, "A two directional electrostatic comb-drive X-Y micro-stage for MOEMS", Sensors and Actuators A, 163, 255-265, 2010.
doi: 10.1016/j.sna.2010.06.020

[28] B. Verdin, P. Le Moal, G. Bourbon, V. Walter, "Electromechanical Coupling between Comb-Drive Actuators and Charge Pump Converters," Procedia Engineering, Volume 168, pp. 1667-1670, ISSN 1877-7058, 2016.
doi: 10.1016/j.proeng.2016.11.486.